Front. Mech. Eng. 2018, 13(3): 376–384
https://doi.org/10.1007/s11465-018-0500-3

RESEARCH ARTICLE

Ke WEI, Xiaoguang FAN, Mei ZHAN, Miao MENG

Robust optimization of the billet for isothermal local loading transitional region of a Ti-alloy rib-web component based on dual-response surface method

Abstract Billet optimization can greatly improve the forming quality of the transitional region in the isothermal local loading forming (ILLF) of large-scale Ti-alloy rib-web components. However, the final quality of the transitional region may be deteriorated by uncontrollable factors, such as the manufacturing tolerance of the preforming billet, fluctuation of the stroke length, and friction factor. Thus, a dual-response surface method (RSM)-based robust optimization of the billet was proposed to address the uncontrollable factors in transitional region of the ILLF. Given that the die underfilling and folding defect are two key factors that influence the forming quality of the transitional region, minimizing the mean and standard deviation of the die underfilling rate and avoiding folding defect were defined as the objective function and constraint condition in robust optimization. Then, the cross array design was constructed, a dual-RSM model was established for the mean and standard deviation of the die underfilling rate by considering the size parameters of the billet and uncontrollable factors. Subsequently, an optimum solution was derived to achieve the robust optimization of the billet. A case study on robust optimization was conducted. Good results were attained for improving the die filling and avoiding folding defect, suggesting that the robust optimization of the billet in the transitional region of the ILLF was efficient and reliable.

Keywords isothermal local loading forming, rib-web component, transitional region, robust optimization, dual response surface method

1 Introduction

Large-scale titanium alloy rib-web components (LTRCs), which can satisfy the demands of high-efficiency structures and lightweight materials, have been extensively applied in the aviation and aerospace industries [1–3]. However, such components are difficult to fabricate through traditional forging technology because of the complex structure of large-size components and difficulty in deforming titanium alloy. Isothermal local loading forming (ILLF) is an advanced manufacturing technology that integrates the advantages of local loading and isothermal forming, thereby providing a feasible way to manufacture these components [4–6]. ILLF is an isothermal forming process under a local loading condition, in which the load is applied to the local region of the billet, as shown in Fig. 1. Integral components can be formed by changing the loading regions individually. This process can reduce the loading regions in integral components and enlarge the component size.

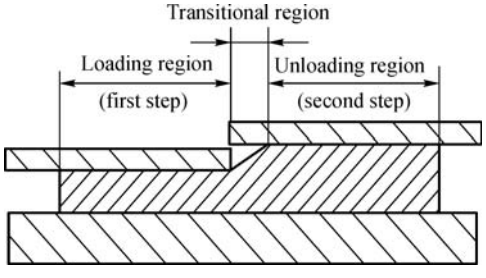

Fig. 1 Illustration of the local loading forming

The ILLF technology comprises three regions, i.e., loading, unloading, and transitional regions, which are illustrated in Fig. 1. Gao et al. [7,8] pointed out that the material in the transitional region undergoes highly complex unequal deformation and material flow, which may cause folding defect and die underfilling. Thus, the

Received July 27, 2017; accepted October 11, 2017

Ke WEI, Xiaoguang FAN (✉), Mei ZHAN, Miao MENG
State Key Laboratory of Solidification Processing, School of Materials Science and Engineering, Northwestern Polytechnical University, Xi'an 710071, China
E-mail: fxg3200@nwpu.edu.cn

transitional region needs more concerns than any other regions. Wei et al. [9] performed 3D finite element (FE) simulation and experiments to analyze the deformation characteristic and possible forming defect in the transitional region, as shown in Fig. 2. Their results revealed that the folding defect occurs in the transitional region during the second-loading step because of the inevitable transfer of the material from the loading to the unloading region. Moreover, die underfilling occurs after the second-loading step in the transitional region because of an improper initial volume distribution, resulting in non-concurrent die filling in the cavities of the ribs. Therefore, folding and die underfilling are two important problems in the transitional region of the LTRC when using the ILLF technology. These problems do not only decrease the accuracy of the component but also weaken the performance of the component. Several studies on the transitional region of the ILLF have been conducted to overcome these problems. Preferable process parameters [8], reasonable volume distribution of the billet [9], and optimal die parameters [10] can avoid folding defect and improve the die filling capability in the transitional region.

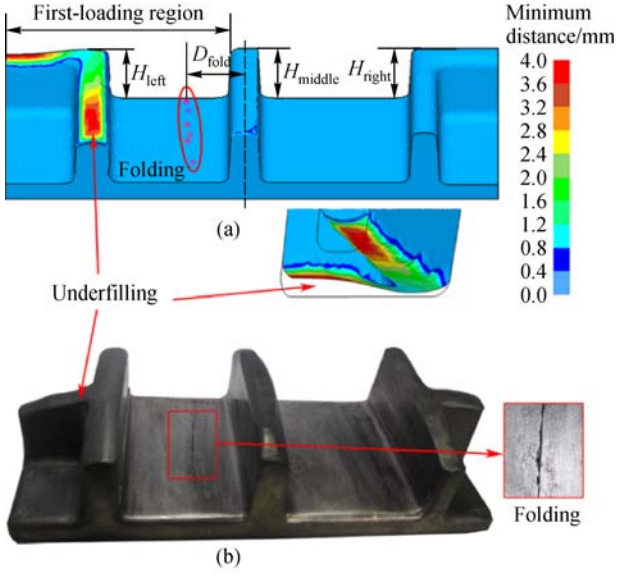

Fig. 2 Folding defect and die underfilling of the transitional region in the ILLF of the LTRC [9]

Nevertheless, for a given optimal forming condition in the actual ILLF process, factors such as the manufacturing tolerance of the preforming billet (MF_{error}), fluctuation of the stroke length (L_{error}), and friction condition (m) can hardly be controlled. These uncontrolled factors are unavoidable in the transitional region, and the folding defect can be induced, the die filling capability can be deteriorated by a combination of these uncontrolled factors. Dr. Taguchi [11] proposed a robust design methodology to minimize the effect of uncontrolled factors and improve product performance. The robust design method has been successfully used in many product design processes [12–14]. Thus, the robust optimization of the billet that considers the uncontrolled factors in the transitional region of the ILLF can improve the forming quality of the LTRC. Because the initial volume distribution plays a key role in folding and die underfilling in the transitional region during the ILLF [9], the present attention is focused on optimizing the billet to improve die filling and avoid folding defect under various combinations of the uncontrolled factors. In this way, the effect of uncontrolled factors on the forming quality of the transitional region can be minimized, and the final quality of the LTRC can be improved.

In this work, the robust optimization of the billet for the transitional region of the ILLF was discussed based on the dual-response surface method (RSM). A case study was conducted on the eigenstructure for the transitional region of the ILLF, and the robust optimization of the billet in the transitional region was achieved. The die underfilling of the transitional region was insensitive to the uncontrolled factors under the constraint condition of avoiding folding defect.

2 Robust optimization steps in the transitional region

2.1 Constructing the cross array

The robust optimization process relies mainly on the experimental data, because the control and uncontrolled factors must be considered [15]. The robust optimization parameters in the transitional region under the ILLF of the LTRC are classified as follows:

1) Control factors ($\boldsymbol{x}$): Control variables $\boldsymbol{x}$ can be exactly controlled and are similar to the design variables used in deterministic optimization. In this work, the design variables were the size parameters of the billet, which could be used to adjust the volume distribution in the transitional region. An unequal-thickness billet (UTB) was adopted because it can adjust the volume distribution at a low cost and high efficiency [16,17]. The geometry of the UTB and corresponding size parameters are shown in Fig. 3.

2) Uncontrolled factors ($\boldsymbol{Z}$): Variables $\boldsymbol{Z}$ cannot be controlled by the designer, or their settings are difficult or costly to control. These variables are also called noise factors, which are often caused by the operating environment, machine accuracy, and manufacturing tolerance. These uncontrolled factors may deteriorate the forming quality and lead to product failure.

3) Responses ($\boldsymbol{Y}$): Responses are the objective functions, which are expressed as the mean and standard deviation of the die filling capability in the transitional region.

After the control and uncontrolled factors were identified, the control factors were arranged in the outer array,

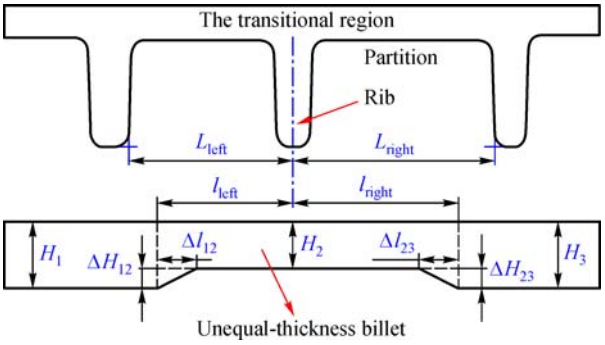

Fig. 3 Illustration of the UTB and size parameters

whereas the uncontrolled factors were arranged in the inner array. The cross array was then constructed to locate the sampling points for the response of the objective function [15], as shown in Table 1.

Table 1 Cross array with control and uncontrolled factors

Control factors				Uncontrolled factors				
Outer array				Inner array				
				Z_1	1	1	…	3
				Z_2	1	2	…	3
				Z_3	1	2	…	2
				Z_4	1	2	…	1
x_1	x_2	x_3	x_4					
1	1	2	3		$f_{1,1}$	$f_{1,2}$	…	$f_{1,j}$
1	2	3	2		$f_{2,1}$	$f_{2,2}$	…	$f_{2,j}$
1	3	1	1		$f_{3,1}$	$f_{3,2}$	…	$f_{3,j}$
…	…	…	…		…	…	…	…
1	2	2	2		$f_{i,1}$	$f_{i,2}$	…	$f_{i,j}$

FE simulation was incorporated to simulate the process in the transitional region of the ILLF. $f_{i,j}$ is the die underfilling rate at the ith row of the outer array and the jth column of the inner array. $f_{i,j}$ can be expressed as

$$f_{i,j} = [(V_{\text{eigen}} - V_{\text{actual}})/V_{\text{eigen}}] \times 100\%, \quad (1)$$

where V_{actual} is the actual volume of the eigenstructure when a certain rib (the partition rib, the rib in the first-loading region or in the second-loading region) of the transitional region is fully filled before any other ribs during the second-loading step. To facilitate good comparability for the die filling capability with different volume distributions, the corresponding material volume of the remaining reduction amount was cut when the stroke of the top die was unfinished at that moment.

2.2 Dual-RSM modeling

After all the FE simulations in the cross array were completed, the mean and standard deviation of the die underfilling rate ($f_{i,j}$) were calculated under each row of the outer array using the following equation:

$$f_i^{\mu} = \frac{1}{n}\sum_{j=1}^{n} f_{i,j}, \quad (2)$$

$$f_i^{\sigma} = \sqrt{\frac{1}{n-1}\sum_{j=1}^{n}(f_{i,j} - f_i^{\mu})^2}, \quad (3)$$

where f_i^{μ} and f_i^{σ} are the mean and standard deviation of the response at the i sampling point in the outer array, and n is the number of the sampling points in the inner array. Dual-RSM [12,18] was adopted by considering the mean and standard deviation of the die underfilling rate. Subsequently, the dual-RSM model of f_i^{μ} and f_i^{σ} was constructed via stepwise regression method with the following equation:

$$y = \beta_0 + \sum_{j=1}^{k}\beta_j x_j + \sum_{j=1}^{k}\beta_{jj} x_j^2 + \sum_{i=1}^{k-1}\sum_{j=i+1}^{k}\beta_{ij} x_i x_j, \quad (4)$$

where y is the response of f_i^{μ} or f_i^{σ}, k is the number of input variables, x_i and x_j are the set of model input variables, and β_0, β_j, β_{jj}, and β_{ij} represent the regression coefficients.

2.3 Constraint condition

Previous studies on ILLF revealed that the folding defect in the transitional region is one of the most important factors that influence the forming quality of the LTRC [7–9]. Thus, avoiding folding defect in the transitional region is crucial to the integral component. Previous studies also found that the severity of the folding defect is well correlated with the quantity of material transferred to the first-loading region during the second-loading step. Meanwhile, increasing the friction can decrease the quantity of the transferred material. During the local loading forming process, the friction factor may be varied by changing the lubrication status and die surface roughness. Thus, folding defect caused by friction fluctuation must be avoided. In view of the safety margin in engineering applications, the lowest friction factor within its fluctuation range was chosen for determining the critical value of the material transfer percentage (M_t) in the robust optimization process. M_t can be expressed as follows:

$$M_t = [(V_n - V_f)/V_{\text{eigen}}] \times 100\%, \quad (5)$$

where V_n is the volume of the workpiece in the first-loading region when a neutral layer is formed in the web of the first-loading region (close to the partition rib) during the second-loading step, and V_f is the volume of the workpiece in the first-loading region after the first-loading step. The critical value of M_t is a constraint condition in the

robust optimization process, and it can be obtained by stepwise decreasing the reduction amount in the equal-thickness billet [9]. If M_t is less than or equal to the critical value, then no folding defect is produced in the transitional region. By contrast, when M_t is greater than the critical value, then a folding defect is produced.

2.4 Robust optimization solution

The robust optimization of the billet can be attained by a constrained nonlinear programming algorithm, which combines the results of the dual-RSM model and constraint condition. The flowchart of the robust optimization of the billet in the transitional region during the ILLF of LTRC is shown in Fig. 4.

3 Case study

3.1 FE modeling

On the basis of the local loading feature [6], a typical eigenstructure was selected for the case study to illustrate the robust optimization steps, as shown in Fig. 5. The geometric parameters of the eigenstructure are listed in Table 2. In view of the symmetrical feature of the eigenstructure in the center of the two transverse ribs (Ribs 4 and 5), half of the eigenstructure was chosen for the FE model to enhance the simulation accuracy and reduce the simulation time. The combined die structure and billet geometry of the FE model were established under the DEFORM-3D environment, as shown in Fig. 6. To attain the local loading condition, the bottom die was divided into bottom Dies 1 and 2. The die partition line was located on the middle rib (Rib 2) of the eigenstructure. During the first-loading step, a spacer block was inserted under bottom Die 1 to adjust the relative position of the two bottom dies, as shown in Fig. 6(a). In this situation, the load was exerted only in the first-loading region. In the second-loading step (Fig. 6(b)), the spacer was removed, so bottom Dies 1 and 2 were at the same horizontal level, and the load was exerted only in the second-loading region. In this way, ILLF technology could be applied to depict a local loading condition by a one-single action hydraulic press.

In this work, robust optimization was performed with an FE simulation-based approach. Thus, the key technologies of FE modeling are listed to provide a complete understanding of the FE model.

1) The material of the workpiece is TA15 titanium alloy, for which the flow stress constitutive equation was determined by using stress-strain curves [19]. The material was defined as a homogeneous and incompressible body. The von Mises yielding criteria and the isotropic hardening rule were adopted.

2) The local loading forming of the rib-web component was a typical bulk forming process, such that the elastic deformation of the workpiece was neglected, and the rigid visco-plastic FE method was employed.

3) The thermal events were neglected during the local loading process under the isothermal condition and low loading speed.

4) A constant shearing friction model was used to describe the friction behavior between the workpiece and dies.

5) The workpiece was discretized by tetrahedral elements, and the initial average mesh size was approximately 1/5 of the width of the ribs. To maintain a high-quality mesh and enhance the calculation efficiency, remeshing and local refined meshing technologies were adopted to reduce element distortion.

6) The deformation temperature and loading speed of the top die were set to 970 °C and 0.02 mm/s, respectively.

7) Multi-pass local loading forming is inconvenient to the production process and may result in poor microstructure and performance for the LTRC [7]. Thus, only one local loading pass was fixed for the eigenstructure in this work.

In addition, the values of the spacer block (H_{sb}= 14 mm) and the fillet radii of the die (R = 5 mm) were selected based on the recommended values of Gao et al. [8,10]. In a previous work [9], the developed 3D-FE model was verified to be reliable in predicting the position of the folding and height of the ribs in the transitional region through a physical experiment, as shown in Fig. 2. These findings suggest that the established 3D-FE model presented a high prediction accuracy and provided the essential data for the dual-RSM model and constraint condition under different UTBs.

3.2 Construction of the dual-RSM model

In the current study, the size parameters h_1, h_3, l_{left}, and l_{right} in Fig. 3 were regarded as design variables for adjusting the volume distribution of the billet in the transitional region. Accordingly, the corresponding values H_1/H_e, H_3/H_e, l_{left}/L_{left}, and l_{right}/L_{right} were considered the control factors a, b, c, and d. It is noted that the total volume of the different UTBs was maintained constant by complying with the constant-volume principle. H_2 was set as a dependent variable by changing the design variables. During the forming process of the ILLF, the stroke length (L_{error}) may be also fluctuated, because the bottom die center accuracy of the press would be decreased by the installation accuracy and block vibration. Thus, the nominal stroke may not be attained. Moreover, the existing manufacturing tolerance of the preforming billet (MF_{error}) in the operating environment can influence the precision of the volume distribution, resulting in distinct forming results in the transitional region in the ILLF of the LTRC. Therefore, MF_{error}, m, and L_{error} were regarded as

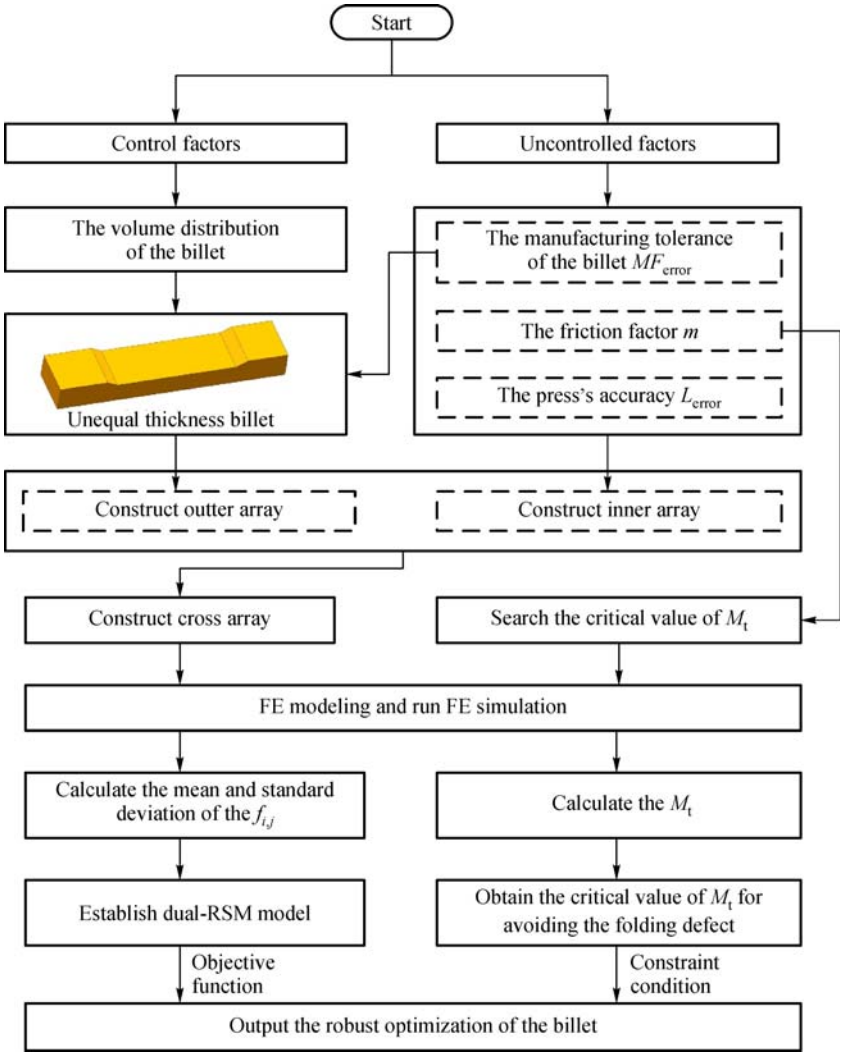

Fig. 4 Flowchart of the robust optimization of the billet in the transitional region during the ILLF of LTRC

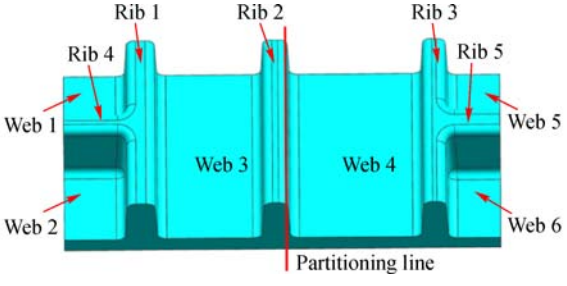

Fig. 5 Eigenstructure of the transitional region

uncontrolled factors. The ranges of the control and uncontrolled factors are listed in Table 3. The control factors were arranged in the outer array using Box-Behnken design (BBD), whereas the uncontrolled factors were arranged in the inner array using the uniform design (UD). The designed cross array is shown in Table 4.

Each experiment from the outer array was repeated five times (Column $j = 5$) with different parameters of the inner array. The mean (f^{μ}) and standard deviation (f^{σ}) of the 29 BBD schemes (Row $i = 29$) were calculated using Eqs. (2) and (3). Subsequently, the dual-RSM model was used to predict the relationship of the control factors with f^{μ} and f^{σ}, as shown in Eqs. (6) and (7).

$$f^{\mu} = 24.69918 - 23.40082a - 18.04425b - 9.19271c - 37.56382ab + 8.14694ac + 24.66357a^2 + 32.08279b^2, \quad (6)$$

Table 2 Geometric parameters of the eigenstructure

Feature	Parameter	Value
Rib 1	Width, W_1/mm	15
	Height, H_1/mm	44
Rib 2	Width, W_2/mm	13
	Height, H_2/mm	43
Rib 3	Width, W_3/mm	12
	Height, H_3/mm	45
Rib 4	Width, W_4/mm	12
	Height, H_4/mm	44
Rib 5	Width, W_5/mm	16
	Height, H_5/mm	45
Distance to the left side of Rib 1	D_{01}/mm	35
Distance between Ribs 1 and 2	D_{12}/mm	60
Distance between Ribs 2 and 3	D_{23}/mm	75
Distance to the right side of Rib 3	D_{30}/mm	30
Thickness of Web 1	T_{web1}/mm	13
Thickness of Web 2	T_{web2}/mm	13
Thickness of Web 3	T_{web3}/mm	14
Thickness of Web 4	T_{web4}/mm	14
Thickness of Web 5	T_{web5}/mm	12
Thickness of Web 6	T_{web6}/mm	12
All fillet radii	R/mm	5
All drafts	γ/(°)	2
Width of the eigenstructure	W_{eigen}/mm	100
Volume of the eigenstructure	V_{eigen}/mm^3	5.63×10^5

$$f^{\sigma} = 10.61595 - 8.89809a - 13.41992b + 0.15142c + 2.64596ab - 1.82579ac + 3.60745a^2 + 6.19163b^2 + 1.20071c^2. \quad (7)$$

The significance of the dual-RSM model was assessed by regression analysis. The adjusted R^2 value of 0.9627 (f^{μ}) and 0.9611 (f^{σ}) indicated that the fit of the dual-RSM model was very good, suggesting that the dual-RSM model could be used for the robust optimization of the billet.

3.3 Constraint condition

As mentioned in Section 2.3, a friction factor of 0.3 was chosen for determining the critical value of M_t. Similar to the work in Ref. [9], the critical value of M_t was set to 5.21. The RSM model of M_t ($m = 0.3$) was expressed by Eq. (8), which was fitted by stepwise regression to improve the predictive accuracy. The adjusted R^2 value of 0.9826 indicated that the fit of the RSM model of M_t ($m = 0.3$) was very good. For comparison, the RSM model of M_t ($m = 0.5$) [9] is given in Eq. (9).

$$M_t(m=0.3) = 0.86562 + 13.13201a - 1.80017b - 2.27317c + 4.01580d - 4.90145ab + 2.63536ac - 6.66173a^2 + 3.14348b^2 - 2.39176d^2, \quad (8)$$

$$M_t(m=0.5) = -2.86361 + 7.12846a + 9.84596b - 2.49595c + 4.24479d - 6.14361ab + 2.44892ac - 1.92904bd - 2.96887a^2 - 1.41188b^2 - 1.39701d^2. \quad (9)$$

3.4 Robust optimization solving and discussion

To achieve robust optimization of the billet, the mean and standard deviation of the die underfilling rate should be minimized. The critical value of M_t under $m = 0.3$ and $m = 0.5$ were considered in the constraint condition for avoiding folding defects in the robust optimization

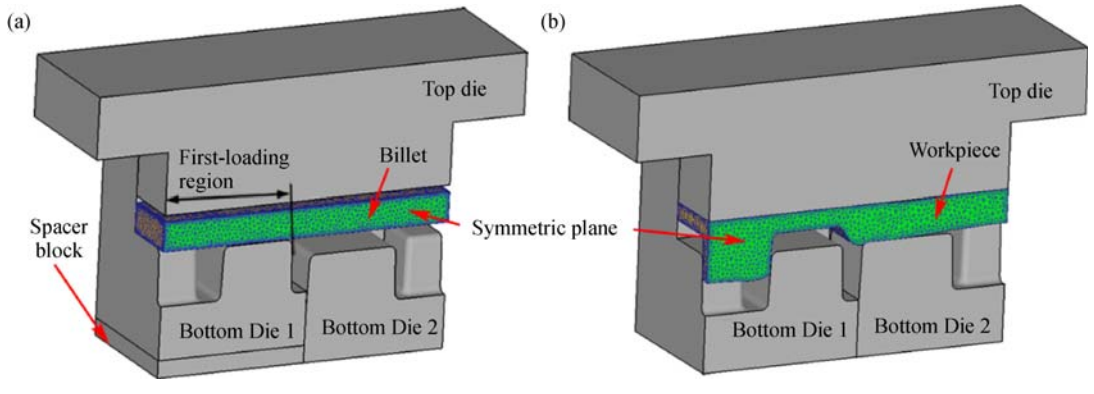

Fig. 6 FE model in the transitional region of ILLF [9]. (a) First-loading step; (b) second-loading step

Table 3 Ranges of the control and uncontrolled factors

Factor type	Variables	Minimum values	Maximum values
Control factors	a: H_1/H_e	0.75	1.15
	b: H_3/H_e	0.75	1.15
	c: l_{left}/L_{left}	0.60	1.00
	d: l_{right}/L_{right}	0.60	1.00
Uncontrolled factors	MF_{error}	−0.1 mm	0.1 mm
	m	0.3	0.5
	L_{error}	13.9 mm	14 mm

process. By combining the objective function and constraint condition, the robust optimization model was formulated in Eq. (10).

$$\left.\begin{aligned} &\text{Variables} && a,b,c,d \\ &\text{Minimum} && f^{\mu}+f^{\sigma} \\ &\text{s.t.} && M_t(m=0.3)\leqslant 5.21 \\ & && M_t(m=0.5)\leqslant 4.24 \\ & && 0.75\leqslant a,\ b\leqslant 1.15 \\ & && 0.6\leqslant c,\ d\leqslant 1 \end{aligned}\right\} \tag{10}$$

Table 4 Cross array design

BBD NO.	Control factors				Uncontrolled factors						Responses	
					UD	1	2	3	4	5		
					MF_{error}	−0.10	−0.05	0.00	0.05	0.10	f_i^{μ}	f_i^{σ}
					m	0.35	0.45	0.30	0.40	0.50		
	a	b	c	d	L_{error}	13.975	13.950	13.925	13.900	14.000		
1	1.15	0.95	0.8	0.6		1.29	1.32	1.49	1.30	1.58	1.40	0.13
2	0.95	1.15	0.8	0.6		4.30	5.24	4.00	5.06	5.32	4.78	0.59
3	0.75	0.95	0.6	0.8		4.88	4.93	4.07	4.82	5.07	4.75	0.39
4	1.15	1.15	0.8	0.8		1.84	2.58	1.30	2.60	2.34	2.13	0.56
5	0.95	0.95	1.0	1.0		1.23	1.39	1.12	1.12	1.62	1.29	0.21
6	0.95	0.95	0.8	0.8		1.43	1.48	1.27	1.30	1.65	1.43	0.15
7	1.15	0.95	1.0	0.8		1.22	1.13	1.29	1.04	0.92	1.12	0.15
8	0.95	0.95	0.6	0.6		1.73	1.35	1.55	1.52	1.59	1.55	0.14
9	0.95	0.95	0.6	1.0		1.51	1.28	1.52	1.54	1.62	1.49	0.13
10	0.75	0.95	1.0	0.8		2.20	2.58	2.08	3.25	3.79	2.78	0.73
11	0.95	1.15	0.6	0.8		3.95	4.82	3.46	4.29	4.77	4.26	0.57
12	0.95	0.75	0.6	0.8		1.35	1.80	1.35	1.42	1.24	1.43	0.21
13	0.75	0.95	0.8	0.6		2.91	3.46	2.69	3.69	3.85	3.32	0.50
14	0.75	0.95	0.8	1.0		3.48	3.96	3.23	4.23	4.41	3.86	0.50
15	0.95	0.95	0.8	0.8		1.59	1.25	1.37	1.30	1.63	1.43	0.17
16	0.95	0.75	0.8	1.0		1.35	1.49	1.10	1.53	1.05	1.30	0.22
17	0.95	0.95	0.8	0.8		1.56	1.60	1.32	1.32	1.59	1.48	0.15
18	1.15	0.95	0.8	1.0		1.23	1.26	1.35	1.34	1.52	1.34	0.11
19	1.15	0.75	0.8	0.8		2.76	2.81	2.63	2.59	2.79	2.72	0.10
20	0.95	0.75	1.0	0.8		1.21	1.14	1.03	1.35	0.57	1.06	0.30
21	0.95	0.75	0.8	0.6		1.35	1.54	1.24	1.46	1.01	1.32	0.21
22	0.75	0.75	0.8	0.8		1.96	1.97	0.97	2.81	2.42	2.03	0.69
23	0.95	1.15	1.0	0.8		4.14	5.11	3.15	4.93	4.66	4.40	0.79
24	0.95	0.95	0.8	0.8		1.45	1.21	1.42	1.36	1.61	1.41	0.15
25	0.95	0.95	0.8	0.8		1.46	1.23	1.40	1.32	1.63	1.41	0.15
26	0.95	1.15	0.8	1.0		3.92	4.60	3.34	4.42	4.63	4.18	0.55
27	1.15	0.95	0.6	0.8		1.67	1.73	1.76	1.89	1.91	1.79	0.11
28	0.75	1.15	0.8	0.8		7.05	8.20	6.42	7.59	7.99	7.45	0.73
29	0.95	0.95	1.0	0.6		1.03	1.20	1.21	1.37	0.87	1.14	0.19

Table 5 Comparison between robust optimization and deterministic optimization

Optimization type	a	b	c	d	f_i^{μ}	f_i^{σ}
Robust optimization	1.12	0.93	0.65	1	1.23	0.09
Deterministic optimization	1.13	0.96	1.00	1	1.26	0.15

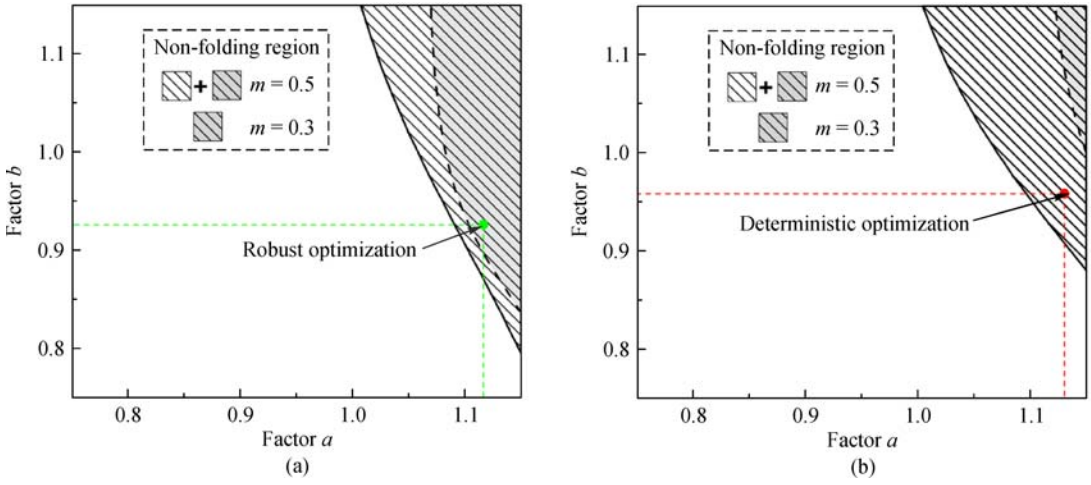

Fig. 7 Contour graphs demonstrating the effects of Factors a and b on M_t. (a) Factor $c = 0.65$, Factor $d = 1$; (b) Factor $c = 1$, Factor $d = 1$

An optimum solution was derived to attain the robust optimization of the billet using MAPLE software. The results of the robust optimization are given in Table 5. The corresponding mean and standard deviation values of the die underfilling rate were 1.23 and 0.09, respectively. To better understand the robust optimization effect, the deterministic optimization of the billet, which considered neither the manufacturing tolerance of the billet nor the fluctuation of the friction factor and stroke length (the friction factor was set to 0.5, and the stroke length was fixed at 14 mm) was also obtained. The forming results indicated that both the mean and standard deviation of the die underfilling rate were greater than the robust optimization outcomes, as shown in Table 5. Thus, the robust optimization of the billet in this case was efficient and reliable.

Figure 7 compares the folding results between the robust optimization point and deterministic optimization point by showing the contour plots of Eqs. (8) and (9). The robust optimization point that considered the constraint condition is illustrated in Fig. 7(a). The robust optimization point was included in the non-folding region of both $m = 0.3$ and $m = 0.5$. However, the deterministic optimization point in Fig. 7(b) was only included in the non-folding region of $m = 0.5$ but outside of the non-folding region of $m = 0.3$. In addition, the FE simulation result of the deterministic optimization revealed that folding was produced under a friction factor $m = 0.3$, further demonstrating that the fluctuation of the friction factor significantly influenced the folding defect. Thus, it is concluded that the folding defect caused by the fluctuation of the friction factor was effectively avoided by the robust optimization result.

4 Conclusions

In this study, a dual-RSM-based robust optimization of the billet in the transitional region of LTRC under the ILLF was developed to improve the die underfilling rate under the constraint condition of avoiding folding defect. The uncontrollable factors (i.e., the manufacturing tolerance of the performing billet, fluctuation of the stroke length, and friction factor) were considered in the robust optimization process. A case study of a typical rib-web eigenstructure was implemented to demonstrate the effectiveness of the robust optimization method. BBD and UD were adopted during dual-RSM metamodeling to acquire the mean and standard deviation of the die underfilling rate while considering the size parameters of the UTB and the uncontrollable factors. The constraint condition of avoiding folding defect in the robust optimization process was determined in terms of the fluctuation of the friction factor. The robust optimization results showed that the mean and standard deviation of the die underfilling rate were both minimized compared with the deterministic optimization results. Thus, the preferable die filling could be acquired in the transitional region of the ILLF by considering the uncontrollable factors and the folding defect caused by the fluctuation of the friction was effectively avoided. The results of the case study demonstrated that the robust

optimization of the billet was critical for improving the forming quality of the transitional region in the ILLF of the LTRC.

Acknowledgements The authors would like to gratefully acknowledge the support given by the National Natural Science Foundation of China (Grant No. 51575449), Research Fund of the State Key Laboratory of Solidification Processing (NWPU), China (Grant No. 104-QP-2014), 111 Project (Grant No. B08040), and Fundamental Research Funds for the Central Universities (Grant No. 3102015AX004).

References

1. Yang H, Fan X G, Sun Z C, et al. Recent developments in plastic forming technology of titanium alloys. Science China. Technological Sciences, 2011, 54(2): 490–501
2. Kleiner M, Geiger M, Klaus A. Manufacturing of lightweight components by metal forming. CIRP Annals-Manufacturing Technology, 2003, 52(2): 521–542
3. Fan X G, Yang H, Gao P F. Through-process macro-micro finite element modeling of local loading forming of large-scale complex titanium alloy component for microstructure prediction. Journal of Materials Processing Technology, 2014, 214(2): 253–266
4. Yang H, Gao P F, Fan X G, et al. Some advances in plastic forming technologies of titanium alloys. Procedia Engineering, 2014, 81: 44–53
5. Yang H, Fan X G, Sun Z C, et al. Some advances in local loading precision forming of large scale integral complex components of titanium alloys. Materials Research Innovations, 2011, 15(Supp1 s1): s493–s496
6. Sun Z C, Yang H, Sun N G. Effects of parameters on inhomogeneous deformation and damage in isothermal local loading forming of Ti-alloy component. Journal of Materials Engineering and Performance, 2012, 21(3): 313–323
7. Gao P F, Yang H, Fan X G, et al. Quick prediction of the folding defect in transitional region during isothermal local loading forming of titanium alloy large-scale rib-web component based on folding index. Journal of Materials Processing Technology, 2015, 219: 101–111
8. Gao P F, Yang H, Fan X G, et al. Forming defects control in transitional region during isothermal local loading of Ti-alloy rib-web component. International Journal of Advanced Manufacturing Technology, 2015, 76(5–8): 857–868
9. Wei K, Zhan M, Fan X G, et al. Unequal-thickness billet optimization in transitional region during isothermal local loading forming of Ti-alloy rib-web component using response surface method. Chinese Journal of Aeronautics, 2017. https://doi.org/10.1016/j.cja.2017.07.005
10. Gao P F, Li X D, Yang H, et al. Improving the process forming limit considering forming defects in the transitional region in local loading forming of Ti-alloy rib-web components. Chinese Journal of Aeronautics, 2017, 30(3): 1270–1280
11. Taguchi G. Taguchi on Robust Technology Development: Bringing Quality Engineering Upstream. New York: ASME Press, 1993
12. Hou B, Wang W R, Li S H, et al. Stochastic analysis and robust optimization for a deck lid inner panel stamping. Materials & Design, 2010, 31(3): 1191–1199
13. Huang Z L, Wang G, Wei S P, et al. Process improvement in laser hot wire cladding for martensitic stainless steel based on the Taguchi method. Frontiers of Mechanical Engineering, 2016, 11(3): 242–249
14. Li H, Xu J, Yang H, et al. Sequential multi-objective optimization of thin-walled aluminum alloy tube bending under various uncertainties. Transactions of Nonferrous Metals Society of China, 2017, 27 (3): 608–615
15. Li Y Q. Research on six sigma robust optimization of sheet metal forming. Dissertation for the Doctoral Degree. Shanghai: Shanghai Jiaotong University, 2006 (in Chinese)
16. Wei K, Yang H, Fan X G, et al. Unequal thickness billet design for large-scale titanium alloy rib-web components under isothermal closed-die forging. International Journal of Advanced Manufacturing Technology, 2015, 81(5–8): 729–744
17. Zhang D W, Yang H. Metal flow characteristics of local loading forming process for rib-web component with unequal-thickness billet. International Journal of Advanced Manufacturing Technology, 2013, 68(9–12): 1945–1965
18. Huang T L, Song X W, Liu X Y. The multi-objective robust optimization of the loading path in the T-shape tube hydroforming based on dual response surface model. International Journal of Advanced Manufacturing Technology, 2016, 82(9–12): 1595–1605
19. Shen C W. Research on material constitution models of TA15 and TC11 titanium alloys in hot deformation process. Thesis for the Master's Degree. Xi'an: Xi'an Northwestern Polytechnical University, 2007 (in Chinese)